



# Letters

## Compensating Mode Conversion Due to Bend Discontinuities Through Intentional Trace Asymmetry

Xinglong Wu , *Student Member, IEEE*, Flavia Grassi , *Senior Member, IEEE*,  
Paolo Manfredi , *Senior Member, IEEE*, Dries Vande Ginste , *Senior Member, IEEE*,  
and Sergio A. Pignari , *Fellow, IEEE*

**Abstract**—In this letter, a comparative analysis is carried out between the mechanism of mode conversion in differential microstrip lines due to bend discontinuities on one side and trace asymmetry on the other side. With the help of equivalent modal circuits, a theoretical basis is provided for the idea to compensate the undesired common mode (CM), due to the presence of the bend, by intentionally designing asymmetric traces. As an application example, the proposed CM-reduction strategy is used in conjunction with another recently-presented wideband CM suppression filter for differential microstrip lines. It is shown that the proposed solution enhances the overall CM-reduction performance of the filter by some decibels, while preserving its transmission properties.

**Index Terms**—Bend discontinuities, common and differential modes, differential interconnects, mixed-mode S-parameters, mode conversion.

### I. INTRODUCTION

INTRODUCING bend discontinuities into the design of microstrip differential interconnects is often unavoidable because of manufacturing constraints, targeted at meeting the highly dense packaging requirements of modern high-speed electronic circuits. However, it is well known that the presence of traces with different length may significantly degrade the signal integrity and electromagnetic compatibility performance [1]–[4]. Particularly, the undesired conversion of differential mode (DM) into common mode (CM)—theoretically null in ideal differential routing schemes—and vice versa is responsible for radiation to nearby devices, as well as for larger susceptibility. Besides bend discontinuities, such detrimental effects may also occur owing to asymmetries of the two sig-

nal lines with respect to ground, for instance, due to imbalance in the terminal networks (mainly related to component tolerances) [5], [6] and/or to geometrical differences in the line cross section (mainly caused by the manufacturing process) [7].

Unlike the aforementioned previous works, in which the mechanisms of mode conversion due to bend discontinuities and trace asymmetries were investigated separately, this letter presents a systematic and combined analysis between the two phenomena of CM generation. With the help of modal circuits, where the DM-to-CM conversion is modeled by induced voltage and current sources, it is proven that the CM generated by the presence of a bend can be mitigated by intentionally introducing a certain amount of asymmetry between the two traces. The achievable compensation depends on the modal terminal impedances, since the induced CM noise is the superposition of inductive and capacitive contributions that combine differently at the two terminations. Such a novel reduction strategy is effective as long as the lines are electrically short, and it can be used in combination with other filtering techniques available in the literature to enhance their CM-suppression performance. As an illustrative example, the proposed methodology is applied in conjunction with the CM-suppression filter presented in [1], leading to an overall reduction of the CM without sacrificing DM signal transmission.

### II. MODELING MODE CONVERSION DUE TO BEND DISCONTINUITIES

The differential microstrip shown in Fig. 1(a), which is characterized by the presence of a 90° bend discontinuity at its midpoint, is considered in the remainder of this letter. On condition that the bend is electrically short, lumped-parameter models with  $\Pi$  [2], [3] or  $T$  topology [1], [4] are interchangeably exploited in the literature. The obtained two-port network is then cascaded with distributed-parameter transmission-line (TL) models, representing the straight line sections, with the objective of predicting voltages and currents at the terminations of the complete microstrip interconnect.

Without loss of generality, the T-shape equivalent circuit in Fig. 1(b) is adopted here, and by analogy with an electrically short three-conductor TL [8], the corresponding self- and mutual

Manuscript received October 10, 2018; revised January 30, 2019; accepted March 5, 2019. Date of publication April 11, 2019; date of current version April 14, 2020. (Corresponding author: Flavia Grassi.)

X. Wu, F. Grassi, and S. A. Pignari are with the Department of Electronics, Information and Bioengineering, Politecnico di Milano, 20133 Milan, Italy (e-mail: xinglong.wu@polimi.it; flavia.grassi@polimi.it; sergio.pignari@polimi.it).

P. Manfredi is with the Department of Electronics and Telecommunications, Politecnico di Torino, 10129 Turin, Italy (e-mail: paolo.manfredi@polito.it).

D. Vande Ginste is with the Department of Information Technology, Internet Technology and Data Science Lab, Ghent University-imec, 9000 Ghent, Belgium (e-mail: dries.vandeginste@ugent.be).

Color versions of one or more of the figures in this letter are available online at <http://ieeexplore.ieee.org>.

Digital Object Identifier 10.1109/TEMC.2019.2904178

inductances and capacitances are collected in matrix form as

$$\mathbf{L}_b = \begin{bmatrix} L_1 & L_m \\ L_m & L_2 \end{bmatrix}, \mathbf{C}_b = \begin{bmatrix} C_1 & -C_x \\ -C_x & C_2 \end{bmatrix} \quad (1)$$

where  $C_1 = C_{1y} + C_x$  and  $C_2 = C_{2y} + C_x$ .

By virtue of such a matrix representation, the mode conversion arising because of the bend can be studied by introducing CM and DM voltages and currents by means of similarity transformation matrices [9]

$$\begin{bmatrix} V_{\text{CM}} \\ V_{\text{DM}} \end{bmatrix} = \underbrace{\begin{bmatrix} 0.5 & 0.5 \\ 1 & -1 \end{bmatrix}}_{\mathbf{T}_V} \cdot \begin{bmatrix} V_1 \\ V_2 \end{bmatrix}; \quad \begin{bmatrix} I_{\text{CM}} \\ I_{\text{DM}} \end{bmatrix} = \underbrace{\begin{bmatrix} 1 & 1 \\ 0.5 & -0.5 \end{bmatrix}}_{\mathbf{T}_I} \cdot \begin{bmatrix} I_1 \\ I_2 \end{bmatrix} \quad (2)$$

where vectors  $[V_1, V_2]^T$  and  $[I_1, I_2]^T$  collect the physical voltages and currents, whereas  $[V_{\text{CM}}, V_{\text{DM}}]^T$  and  $[I_{\text{CM}}, I_{\text{DM}}]^T$  are their modal counterparts. According to (2), the inductance and capacitance matrices in (1) take the modal form

$$\mathbf{L}_m = \mathbf{T}_V \cdot \mathbf{L}_b \cdot \mathbf{T}_I^{-1} = \begin{bmatrix} L_{\text{CM}} & \Delta L \\ \Delta L & L_{\text{DM}} \end{bmatrix} \quad (3a)$$

$$\mathbf{C}_m = \mathbf{T}_I \cdot \mathbf{C}_b \cdot \mathbf{T}_V^{-1} = \begin{bmatrix} C_{\text{CM}} & \Delta C \\ \Delta C & C_{\text{DM}} \end{bmatrix} \quad (3b)$$

where  $L_{\text{CM}} = (L_1 + L_2 + 2L_m)/4$ ,  $L_{\text{DM}} = L_1 + L_2 - 2L_m$ ,  $\Delta L = (L_1 - L_2)/2$ ,  $C_{\text{CM}} = C_1 + C_2 - 2C_x$ ,  $C_{\text{DM}} = (C_1 + C_2 + 2C_x)/4$ , and  $\Delta C = (C_1 - C_2)/2$ . Hence, the relationships between modal voltages and currents at the external ports of the bend [i.e., ports *a* and *c* in Fig. 1(b)] read

$$\begin{bmatrix} V_{\text{CM}}^c - V_{\text{CM}}^a \\ I_{\text{CM}}^c - I_{\text{CM}}^a \end{bmatrix} + j\omega \begin{bmatrix} 0 & L_{\text{CM}} \\ C_{\text{CM}} & 0 \end{bmatrix} \cdot \begin{bmatrix} V_{\text{CM}}^b \\ I_{\text{CM}}^a + I_{\text{CM}}^c \end{bmatrix} = \begin{bmatrix} \Delta V_{\text{CM}}^a + \Delta V_{\text{CM}}^c \\ \Delta I_{\text{CM}}^b \end{bmatrix} \quad (4a)$$

$$\begin{bmatrix} V_{\text{DM}}^c - V_{\text{DM}}^a \\ I_{\text{DM}}^c - I_{\text{DM}}^a \end{bmatrix} + j\omega \begin{bmatrix} 0 & L_{\text{DM}} \\ C_{\text{DM}} & 0 \end{bmatrix} \cdot \begin{bmatrix} V_{\text{DM}}^b \\ I_{\text{DM}}^a + I_{\text{DM}}^c \end{bmatrix} = \begin{bmatrix} \Delta V_{\text{DM}}^a + \Delta V_{\text{DM}}^c \\ \Delta I_{\text{DM}}^b \end{bmatrix} \quad (4b)$$

where

$$\Delta V_{\text{CM,DM}}^{a,c} = -j\omega \Delta L I_{\text{DM,CM}}^{a,c} \quad (5a)$$

$$\Delta I_{\text{CM,DM}}^b = -j\omega \Delta C V_{\text{DM,CM}}^b \quad (5b)$$

and subscripts *a*, *b*, and *c* refer to the sections indicated in Fig. 1(b). The uncoupled CM and DM quantities in the left-hand side of (4) are coupled through the right-hand side vectors, whose entries (5) play the role of induced voltage and current sources responsible for mode conversion. As a matter of fact, the CM sources in (4a) are proportional to the DM voltages and currents in (4b) through the off-diagonal entries  $\Delta L$  and  $\Delta C$  in (3). The same coefficients relate the DM sources in (4b) to the CM voltages and currents in (4a). It should be noted that these

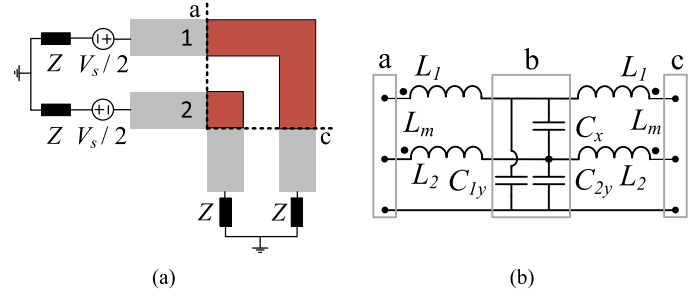


Fig. 1. (a) Differential microstrip structure under analysis. (b) Equivalent circuit model of the bend.

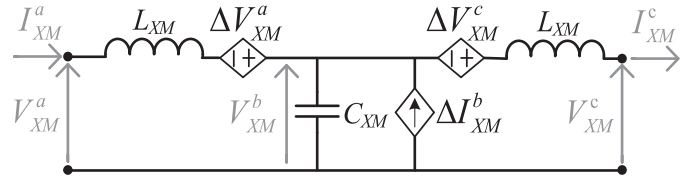


Fig. 2. Circuit interpretation of mode conversion due to bend discontinuities, where *XM* stands for either CM or DM.

coefficients quantify the effect of length imbalance between the two traces, and they would be zero for straight lines, since in that case  $L_1 = L_2$  and  $C_1 = C_2$ . Equations (4) allow for the straightforward circuit interpretation of mode conversion shown in Fig. 2, which is valid both for CM and DM quantities, which have been, therefore, generically denoted with the subscript *XM*.

### III. ANALOGY WITH TRACE ASYMMETRY AND CROSSTALK

As long as the microstrip line is operated according to a differential signaling scheme [i.e., it is fed by an ideal DM source and terminated by perfectly balanced terminal networks, as in Fig. 1(a)], the above analysis can be further simplified by neglecting the back interaction of CM on the DM. Therefore, the induced sources in (4b) are neglected. DM quantities are evaluated first and then used as source terms for the solution of the CM circuit [3]. This uncoupled solution approach, in conjunction with the circuit representation in Fig. 2, allows interpreting the DM-to-CM conversion as the modal counterpart of crosstalk, for which the assumption of weak coupling between the generator and receptor circuits is often exploited to ease the solution [8]. It follows that the undesired CM noise is the superposition of inductive ( $M_{\text{IND}}$ ) and capacitive ( $M_{\text{CAP}}$ ) contributions [8], which are modeled, in the equivalent CM circuit, by induced voltage ( $\Delta V$ ) and current ( $\Delta I$ ) sources that are proportional to the DM currents and voltages, respectively. These sources, lumped in the case of bend discontinuities (see Fig. 2), are distributed (see Fig. 3) in the case of trace asymmetry (and crosstalk), being proportional to the difference between the per-unit-length self-inductances ( $l_1, l_2$ ) and self-capacitances ( $c_1, c_2$ ) associated with the two traces [7].

TABLE I  
ANALOGY BETWEEN BEND DISCONTINUITY, TRACE ASYMMETRY, AND CROSSTALK

	Crosstalk	Trace asymmetry	Bend discontinuity
Source circuit	Generator circuit	DM circuit	
Victim circuit	Receptor circuit	CM circuit	
Coupling coefficients	Mutual inductance/capacitance ( $l_m, -c_m$ )	$\Delta l = (l_1 - l_2)/2$ $\Delta c = (c_1 - c_2)/2$	$\Delta L = (L_1 - L_2)/2$ $\Delta C = (C_1 - C_2)/2$
Induced sources	$\Delta V = -j\omega l_m I_g$ $\Delta I = j\omega c_m V_g$	$\Delta V = -j\omega \Delta l I_{DM}$ $\Delta I = -j\omega \Delta c V_{DM}$	$\Delta V_{CM}^{a,c} = -j\omega \Delta L I_{DM}^{a,c}$ $\Delta I_{CM}^b = -j\omega \Delta C V_{DM}^b$
Superposition at terminations	Left: $\Sigma( M_{IND} ,  M_{CAP} )$ Right: $\Delta( M_{IND} ,  M_{CAP} )$		Left: $\Delta( M_{IND} ,  M_{CAP} )$ Right: $\Sigma( M_{IND} ,  M_{CAP} )$

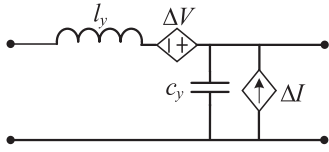


Fig. 3. Model of the victim circuit, where  $y$  stands for either  $m$  (crosstalk) or CM (trace asymmetry).

This is systematically illustrated in Table I, where analytical expressions of the sources induced in the equivalent CM/victim circuits of Fig. 2 (with  $XM = CM$ ) and Fig. 3 are reported in the fourth row. In this analogy, the DM circuit acts as the generator, inducing undesired voltages and currents at the terminations of the CM circuit (the victim) through the imbalance coefficients  $\Delta L$  and  $\Delta C$  (or  $\Delta l$ ,  $\Delta c$ ). These coefficients couple the two modal circuits and play the same role as the mutual inductance and capacitance,  $l_m$  and  $-c_m$  (with  $c_m > 0$ ), play for crosstalk. However, a significant difference is yet to be emphasized. For trace asymmetry, the coupling coefficients are opposite in sign (and likewise for  $l_m$  and  $-c_m$ ), since an increase of the self-inductance corresponds to a decrease of the self-capacitance, and vice versa. On the contrary, in the case of bend discontinuities, they are always concordant, as the difference between self-inductance and self-capacitance results from the length mismatch between the two traces. For instance, for the bend of Fig. 1(a),  $L_1 > L_2$  and  $C_1 > C_2$ , the first line being longer than the second one. This leads to a different combination of inductive  $M_{IND}$  and capacitive  $M_{CAP}$  contributions at the two line ends, as highlighted in the fifth row of Table I, where  $\Sigma$  and  $\Delta$  denote additive and subtractive superposition, respectively. This consideration suggests the possibility to partially compensate the CM generated by the presence of the bend by intentionally introducing a certain amount of asymmetry between the two traces, on condition that one of the two contributions (i.e., inductive or capacitive) is prevailing over the other.

#### IV. INTENTIONALLY ASYMMETRIC BEND

In this section, intentional trace asymmetry is introduced to enhance the performance of the CM filter proposed in [1]. The layout of the filter is shown in Fig. 4. A pair of coplanar microstrips (thickness  $t = 35 \mu\text{m}$  and conductivity  $\sigma = 4.1 \times 10^7 \text{ S/m}$ ) is printed on top of a double-faced printed

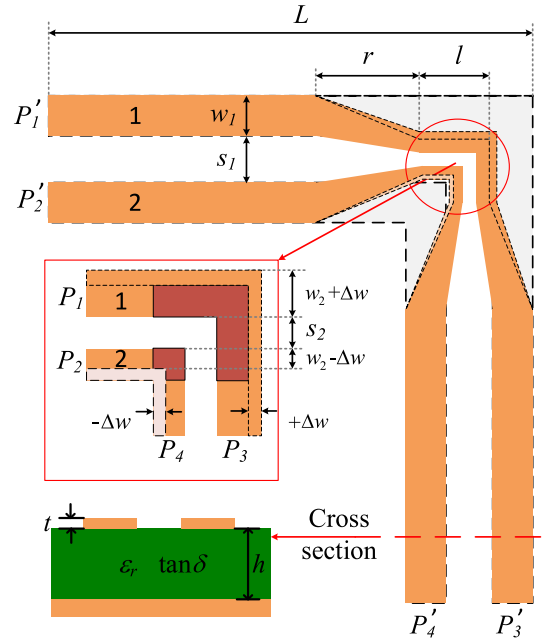


Fig. 4. CM filter under analysis [1] and proposed modification (red square).

circuit board, i.e., a Rogers RO4350B substrate (relative permittivity  $\epsilon_r = 3.66$ , loss tangent  $\tan \delta = 0.003$ , and thickness  $h = 1.524 \text{ mm}$ ). The length of one arm is  $L = 50 \text{ mm}$ , with (original) trace width  $w_1 = 1.8 \text{ mm}$  and spacing  $s_1 = 0.7 \text{ mm}$ . To suppress the CM generated by the bend, a very tightly coupled section is realized with width  $w_2 = 0.3 \text{ mm}$ , spacing  $s_2 = 0.15 \text{ mm}$ , and length  $l = 3 \text{ mm}$  [10]. Transition between the straight arms and the bend is foreseen by means of tapered sections of length  $r = 10 \text{ mm}$ .

##### A. Analysis at the Ports of the Bent Section

A first validation is provided by considering the bent section (i.e., the red area in Fig. 4) only. To this aim, the bend was modeled by the T-shape circuit in Fig. 1(b). Suitable values of the corresponding circuit elements were estimated by the Keysight Advanced Design System (ADS) ‘‘Swept Optimization’’ tool, starting from the S-parameters at the bend ports (i.e., ports  $P_1$ ,  $P_2$ ,  $P_3$ , and  $P_4$  in Fig. 4) computed by full-wave simulation using the ADS Momentum solver [3], [11]. The obtained values

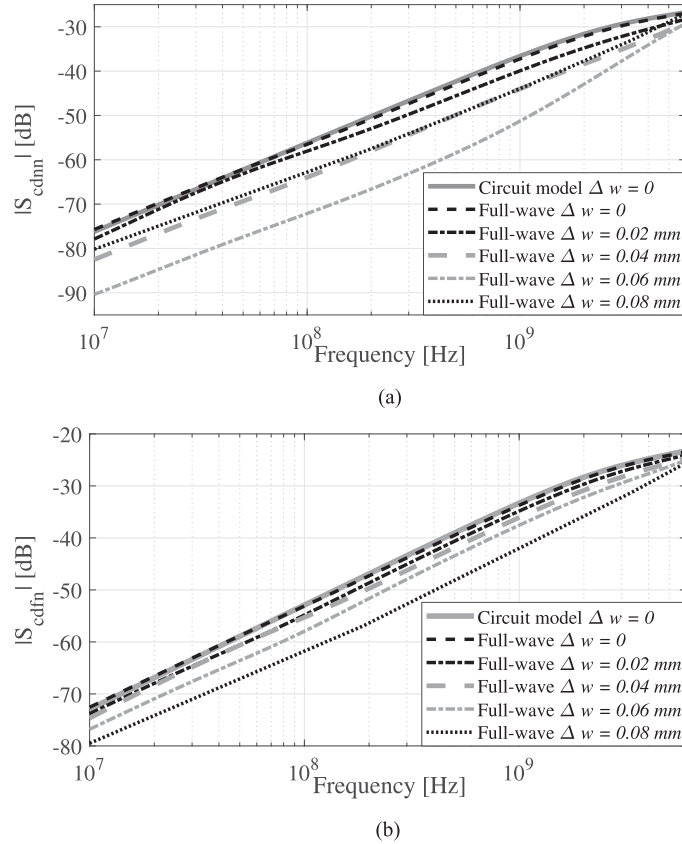


Fig. 5. Magnitude of the DM-to-CM mixed-mode S-parameters at the bend ports ( $P_1$ ,  $P_2$ ,  $P_3$ , and  $P_4$  in Fig. 4). (a) Near end. (b) Far end.

( $L_1 = 0.306$  nH,  $L_2 = 2.562$  pH,  $L_m = 1.543$  pH,  $C_{1y} = 0.056$  pF,  $C_{2y} = 0.010$  pF, and  $C_x = 0.036$  pF) were then cross-validated by comparing the mixed-mode S-parameters of the circuit model (solid gray curves in Fig. 5) versus those originally obtained by full-wave simulation (dashed black curves).

To estimate whether inductive or capacitive coupling is dominant in this specific example, the values of coefficients  $\Delta L = 0.152$  nH and  $\Delta C = 0.023$  pF in (3) are combined with the fact that the relationship between DM voltages and currents is approximately (electrically short TL)  $V_{DM}/I_{DM} = 2Z$ , with  $Z = 50 \Omega$ . As a consequence, based on (5), the equivalent voltage sources  $|\Delta V_{CM}^{a,c}|$  are expected to be nearly hundred times larger than the induced current source  $|\Delta I_{CM}^b|$ , thus indicating the predominant inductive coupling. Accordingly, an asymmetric bend with wider outer trace and thinner inner trace is realized, so that the negative  $\Delta l$  coefficient resulting from this asymmetry can compensate the positive  $\Delta L$  coefficient resulting from the length mismatch.

The sensitivity of mode conversion to the introduced asymmetry can be evaluated in Fig. 5, where the mixed-mode S-parameters obtained by full-wave simulation at the ports of the bent section are plotted for increasing values of width mismatch  $\Delta w$  (see Fig. 4). It is observed that increasing  $\Delta w$  progressively reduces the mode conversion up to a turning point, beyond which the induced CM starts to increase again. This indicates the point at which the inductive coupling becomes

comparable with the capacitive coupling. Since inductive and capacitive coupling combine at the two terminations in a different way, the turning points at the near and far ends are not the same. Hence, to minimize the CM at both ends, the optimum value of  $\Delta w$  has to be generally selected as a tradeoff between the optimal values obtained at the two terminations.

### B. Application to a CM-Suppression Filter

To apply the proposed CM-reduction strategy to the filter of Fig. 4, the theoretical value obtained for  $\Delta w$ , resulting from the sensitivity analysis of Section IV-A, is used as a starting point for further optimization with ADS Momentum. Full-wave simulations of different filter realizations allowed estimating  $\Delta w = 0.03$  mm as the value providing the maximum overall CM reduction at the two terminations in the low-frequency range. Given the almost-linear increase of mode conversion with frequency, the simulations were run for a specific frequency only, namely 1 MHz. Note that for the filter in Fig. 4, a larger  $\Delta w$  also would lead to asymmetric tapered sections, yielding additional undesired CM noise.

The final optimized results are shown in Fig. 6, where the mixed-mode S-parameters obtained by full-wave simulation at the outer ports  $P'_1$ ,  $P'_2$ ,  $P'_3$ , and  $P'_4$  of the differential microstrip line of Fig. 4 are plotted. The solid black curves were obtained for the original microstrip line without a filter [see

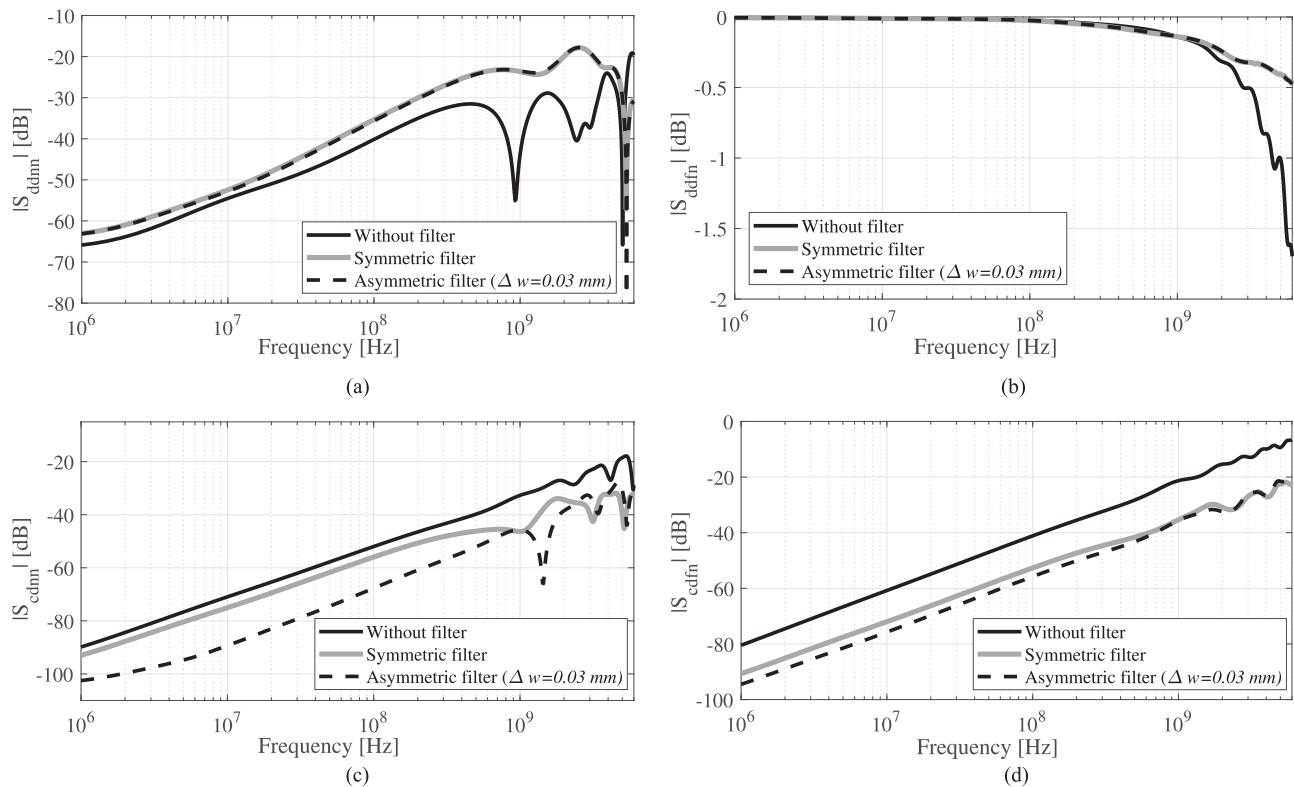


Fig. 6. (a)–(d) Mixed-mode S-parameters at the external ports of the differential microstrip structure under analysis. See text in Section IV-B for details.

Fig. 1(a)]. The solid gray curves were obtained by introducing the original symmetric filter in [1]. Finally, the dashed black curves were obtained by considering the asymmetric filter with  $\Delta w = 0.03$  mm.

The comparison shows that the proposed approach allows enhancing the CM-reduction performance of the filter up to approximately 2.5 GHz. It is also important to mention that the DM performance, in both transmission [see Fig. 6(b)] and reflection [see Fig. 6(a)], remains unaltered over the entire frequency band.

## V. CONCLUSION

This letter investigated the possibility to compensate the undesired mode conversion introduced by bend discontinuities in planar interconnects through the use of intentionally asymmetric traces. To this end, first, suitable DM and CM circuits of the bent section were derived and then used to interpret the resulting mode conversion as the superposition of inductive and capacitive coupling contributions, by analogy with the modeling of crosstalk [8] and mode conversion due to trace asymmetry [7].

The proposed solution is intended to be used in combination with other CM-reduction strategies, without degrading signal transmission. As an explicative example, intentional trace asymmetry was introduced to enhance the performance of the wideband CM filter in [1], leading to an overall CM reduction up to a maximum of 14 dB at low frequency and 30 dB around 1.5 GHz (near-end termination), as proven by full-wave simulations.

## REFERENCES

- [1] C. Gazda, D. Vande Ginste, H. Rogier, R. B. Wu, and D. De Zutter, "A wideband common-mode suppression filter for bend discontinuities in differential signaling using tightly coupled microstrips," *IEEE Trans. Adv. Packag.*, vol. 33, no. 4, pp. 969–978, Nov. 2010.
- [2] G. H. Shiue, W. D. Guo, C. Lin, and R. B. Wu, "Noise reduction using compensation capacitance for bend discontinuities of differential transmission lines," *IEEE Trans. Adv. Packag.*, vol. 29, no. 3, pp. 560–569, Aug. 2006.
- [3] X. Wu, F. Grassi, S. A. Pignari, P. Manfredi, and D. Vande Ginste, "Circuit interpretation and perturbative analysis of differential-to-common mode conversion due to bend discontinuities," in *Proc. IEEE Elect. Des. Adv. Packag. Syst. Symp.*, Haining, China, Dec. 2017, pp. 1–3.
- [4] P. H. Harms and R. Mittra, "Equivalent circuits for multiconductor microstrip bend discontinuities," *IEEE Trans. Microw. Theory Techn.*, vol. 41, no. 1, pp. 62–69, Jan. 1993.
- [5] A. Sugiura and Y. Kami, "Generation and propagation of common-mode currents in a balanced two-conductor line," *IEEE Trans. Electromagn. Compat.*, vol. 54, no. 2, pp. 466–473, Apr. 2012.
- [6] F. Grassi, G. Spadacini, and S. A. Pignari, "The concept of weak imbalance and its role in the emissions and immunity of differential lines," *IEEE Trans. Electromagn. Compat.*, vol. 55, no. 6, pp. 1346–1349, Dec. 2013.
- [7] F. Grassi, Y. Yang, X. Wu, G. Spadacini, and S. A. Pignari, "On mode conversion in geometrically unbalanced differential lines and its analogy with crosstalk," *IEEE Trans. Electromagn. Compat.*, vol. 57, no. 2, pp. 283–291, Apr. 2015.
- [8] C. R. Paul, *Analysis of Multiconductor Transmission Lines*. Hoboken, NJ, USA: Wiley, 2008.
- [9] D. E. Bockelman and W. R. Eisenstadt, "Combined differential and common-mode scattering parameters: Theory and simulation," *IEEE Trans. Microw. Theory Techn.*, vol. 43, no. 7, pp. 1530–1539, Jul. 1995.
- [10] C. Gazda, I. Couckuyt, H. Rogier, D. Vande Ginste, and T. Dhaene, "Constrained multiobjective optimization of a common-mode suppression filter," *IEEE Trans. Electromagn. Compat.*, vol. 54, no. 3, pp. 704–707, Jun. 2012.
- [11] Keysight ADS, Keysight Technologies, Jan. 2016. [Online]. Available: <http://www.keysight.com/en/pc-1297113/advanced-design-system-ads>